JOINT EUROPEAN TORUS JET

JET–P(87)27

K.H. Behringer, W.W. Engelhardt, L. Horton, P.D. Morgan, M.F. Stamp,
H.P. Summers, M. von Hellerman, M.J. Forrest and N.J. Peacock

Status of Visible Spectroscopy on JET

Status of Visible Spectroscopy on JET

K.H. Behringer, W.W. Engelhardt, L. Horton, P.D. Morgan, M.F. Stamp, H.P. Summers[2], M. von Hellerman, M.J. Forrest[1] and N.J. Peacock[1]

JET-Joint Undertaking, Culham Science Centre, OX14 3DB, Abingdon, UK

[1]Culham Laboratory (EURATOM/UKAEA Fusion Association)
[2]On attachment to JET from University of Strathclyde

Preprint of a paper to be submitted for publication in proceedings of
13th Symposium on the Physics of Ionised Gases, Sibenik, Yugoslavia,
1st September - 5th September 1986

XIII SYMPOSIUM ON THE PHYSICS OF IONISED GASES

(Sibenik, Yugoslavia 1-5th Sept 1986)

'STATUS OF VISIBLE SPECTROSCOPY ON JET'

K H Behringer, W W Engelhardt, L Horton, P D Morgan, M F Stamp, H P Summers°, M von Hellerman, P G Carolan*, M J Forrest* and N J Peacock*

JET (Joint European Undertaking), Abingdon, Oxon, OX14 3EA, UK.

* Culham Laboratory (Euratom/UKAEA Fusion Association).

° On attachment to JET from University of Strathclyde.

Abstract

This paper discusses diagnostic information derived from the visible radiation spectrum of JET. Most of the optical line features originate from the relatively cool boundary layer of the tokamak plasma. Their importance stems from the crucial role which the edge plasma appears to play in the overall performance of the tokamak.

Line radiation from the edge plasma is interpreted in terms of influxes of particles from the boundary materials. Using multi-chord viewing of the plasma cross-section, recycling rates, erosion and re-deposition of the elements on different surfaces can be followed. The separate elemental influxes and the composition of the core plasma are related through the release processes from the walls and through cross-field particle transport. Together with the chemical abundances of the ions in the core, the influxes give the global confinement of the elements in the plasma.

Collision processes from the core plasma are also represented in the optical spectrum. These (generally weaker) features include the bremsstrahlung continuum from which the effective ion charge is routinely derived. Forbidden lines due to transitions between levels within the same ground configuration in highly ionised atoms are sometimes observed. Transitions between high quantum (Rydberg) states of plasma ions can be

excited in the visible by charge transfer collisions with energetic beams of injected neutral atoms. The spectral signature of these charge exchange recombination lines in H-like ions uniquely allows the concentration of bare nuclei in the plasma core to be measured.

Diagnostic applications of each of the above features of the optical radiation from JET are described.

I INTRODUCTION

Optical radiation from a tokamak is dominated by collision processes at the relatively cool outer boundary of the plasma. It might be thought therefore that the study of visible radiation has little relevance to the study of multi-keV [1] temperatures plasmas such are produced routinely in the JET device. In recent years, however, the importance of the edge region in determining the global performance of a tokamak has become better appreciated. In the analysis of the physics of the boundary layer the electron temperature $T_e(r)$ and density $n_e(r)$ at the boundary are crucial parameters, which themselves are partly determined by the operational mode of the device, that is to say, whether the plasma has a magnetic flux boundary or is in contact with material limiters, whether the plasma density is maintained by solid pellet refuelling, injection of energetic neutrals or simply recycling of desorbed atoms from the boundary material. Large variations in the global particle and energy confinement are commonly found with different refuelling and other operational scenarios [2][3].

One of the prominent features of the visible emission is the outside annular ring of Balmer emission which from early tokamak studies [4] has been interpreted in terms of an ionisation rate and, therefore, as an influx of electrons and fuel ions. In the case when the only source of electrons S(r) is the ionisation of neutral particles at the plasma edge then,

$$\frac{d\, n_e(r)}{dt} = \frac{1}{r}\frac{d}{dr}\, r\, D_\perp \frac{d\, n_e}{dr} + S(r) \qquad (1)$$

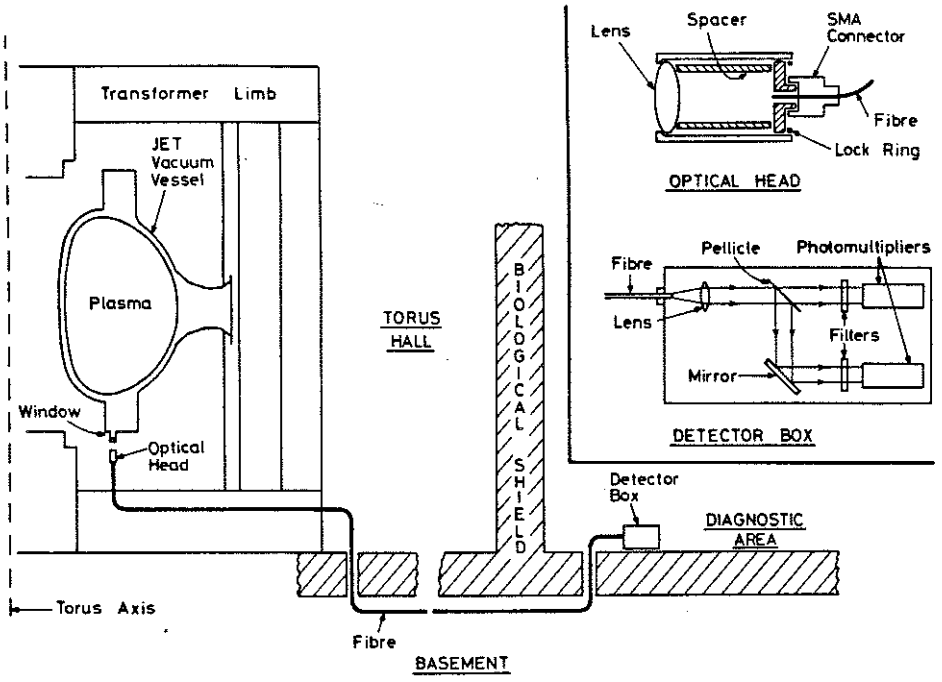

FIGURE 1
Schematic of visible light diagnostic on JET showing, ~100m long, optical fibre link between torus and diagnostic area. Details of the optical head and a dual spectral channel detector arrangement, are shown inset. Typically, many viewing chords are ducted simultaneously to various types of spectral analysers, including spectrometers with optical multichannel analysers (OMA's), in the diagnostic area.

Recombination of effluxing ions does not appreciably add to the boundary emission. If the density and its time derivative can be established, usually by interferometry, so also, from (1) can the particle confinement, with an outflux time characterised by τ_p, viz.,

$$\tau_p = \frac{\bar{n}_e}{\bar{S} - \frac{d\bar{n}_e}{dt}} \qquad (2)$$

The prospect of analysing the Balmer emission was by itself sufficient reason for installing fibre optic conduits [5] see eg, Fig.1, in the early

stages of the diagnostic development programme on JET. As this paper will illustrate, however, the range of applications for these chordal measurements of the visible emission has proliferated and visible spectroscopy is now a much valued diagnostic technique for measuring many aspects of the tokamak performance even into the thermonuclear burn phase of the JET programme.

II The case for developing visible spectroscopy on JET

The following comments are pertinent to the usefulness to JET of visible radiation diagnostics which have often a more limited applicability to other fusion devices.

A plausible steady-state model [6][7][8] for the influx of particles at the plasma boundary assumes that the influx of atoms Γ_A is balanced by the outflow of ions driven by their density gradient $D \frac{\partial n_{A^+}}{\partial r}$ with a solution [9], [10] for the ion density at the plasma edge given by

$$n_A^+ = \Gamma_A \left(\lambda_i \frac{+ \lambda_{sol}}{D}\right) \qquad (3)$$

where λ_i is the ionisation mean free path and λ_{sol}, the "scrape-off layer" thickness, is the e-folding length of the electron density gradient in the shadow of the limiter.

If the same diffusion law applies to impurity atoms as to the hydrogen fuel, then the relative concentrations n_{H°/n_A depends only on their relative influx rates and their respective ionisation mean-free-paths. The latter ratio is a sensitive function of the release energy of the atoms or ions into the plasma. If we postulate that the edge physics parameters such as the density and temperative gradients, sputtering rates, ionisation mean-free-paths etc, are independent of the tokamak size, then the ratio of the line-of-sight radiance due to recycling of atoms at the plasma periphery relative to the chord-integrated emission from high temperative ions in the bulk of the plasma will scale as $(\lambda_i + \lambda_{sol})/a_L$, where a_L is

the minor radius of the toroidal vessel up to the limiter. A tokamak the size of JET R = 3.0m, a_L = 1.25m, b = 2.1m clearly has some advantages over smaller tokamaks in discriminating against edge-produced light when measuring visible continuum and line features emanating from the plasma interior. Other, serendipitous effects can be ascribed to a reduction in wall reflections due to a deliberate blackening (carbonisation) of the walls by glow discharge cleaning in CH_4, the main object of this exercise being a successful, if temporary, reduction in metal influxes. [11].

These factors have led to a progressive upgrading of the diagnostics based on visible spectroscopy as is reflected (Table 1) in the growth in the number of fibre conduits during the operational period 1983-86.

III Optical Fibres Conduits for Visible Radiation

The optical arrangement [5] for relaying visible radiation from JET to the diagnostic area where personnel access is unrestricted is shown in Fig.1. Each optical head is a telescope which views a line-of-sight chord through the plasma. The visible radiation is transmitted via long ~ 100m quartz fibres to a variety of spectroscopic analysers which can be as simple as a filter-photomultiplier, Fig.1, or more elaborately, an échelle spectrometer with 1-D or 2-D photo-detector arrays. Using beam splitters, the output from the fibres is often ducted to several spectrometers each monitoring the absolute emissivity of a different part of the visible spectrum. The lower wavelength limit of the transmission band ~ 3500Å (100m length) is somewhat restrictive in that some of the important atomic lines of Ni I, Fe I, and some of the charge-exchange recombination lines (see later) and the 2271Å line of CV, are occluded.

Sample time-frames of different regions of the spectrum in the proximity of the Balmer lines are shown in Figs.2, 3 and 4. The relative intensities of the Balmer lines can be modelled theoretically [12] provided $n_e(r)$ and $T_e(r)$ are known. Thus an absolute calibration at one wavelength, say H_α, provides a reference influx level with which the other emission lines can be compared.

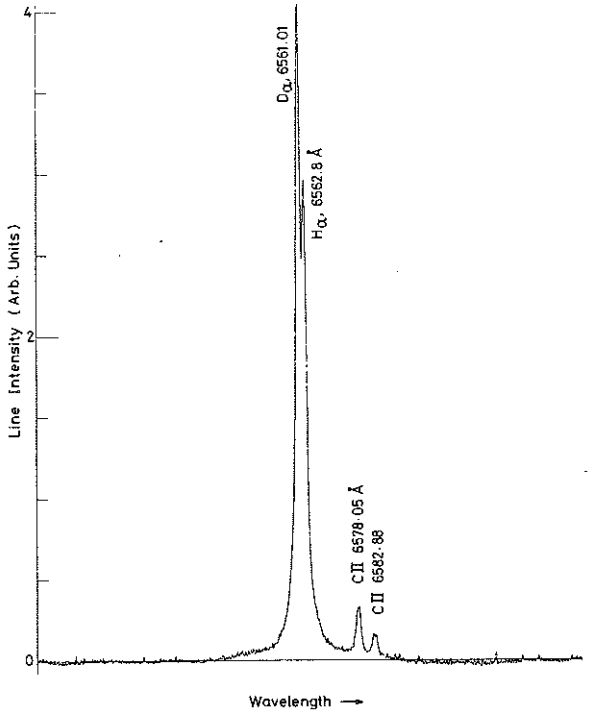

FIGURE 2

Spectrum from JET in the region of Balmer α. The intensity ratio of Hα/Dα and of CII/Dα gives the relative influxes of these species and the relative concentrations of the hydrogen isotopes in the plasma. The spectrum was recorded with the plasma located in the centre of the torus (J #3394).

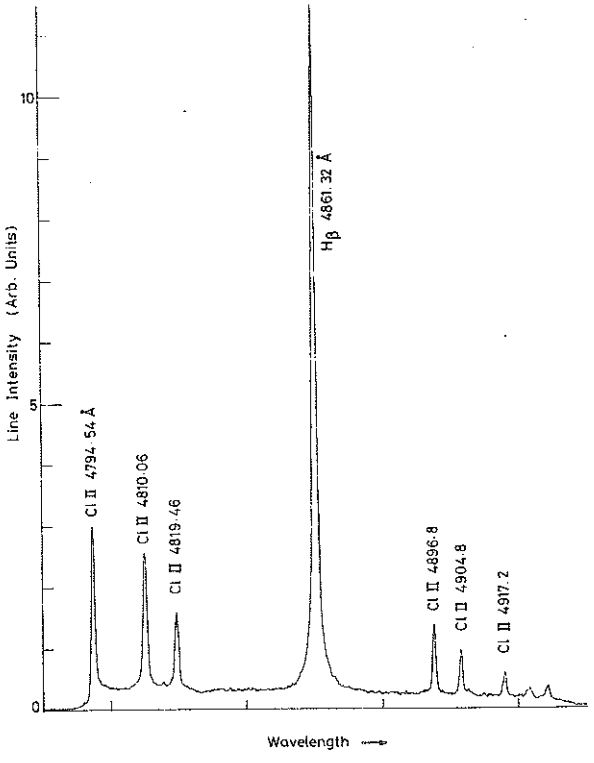

FIGURE 3

Spectrum from JET in the region of Balmer β. The intensities and therefore the influxes of Cl II have been much reduced since this early JET pulse (J # 266).

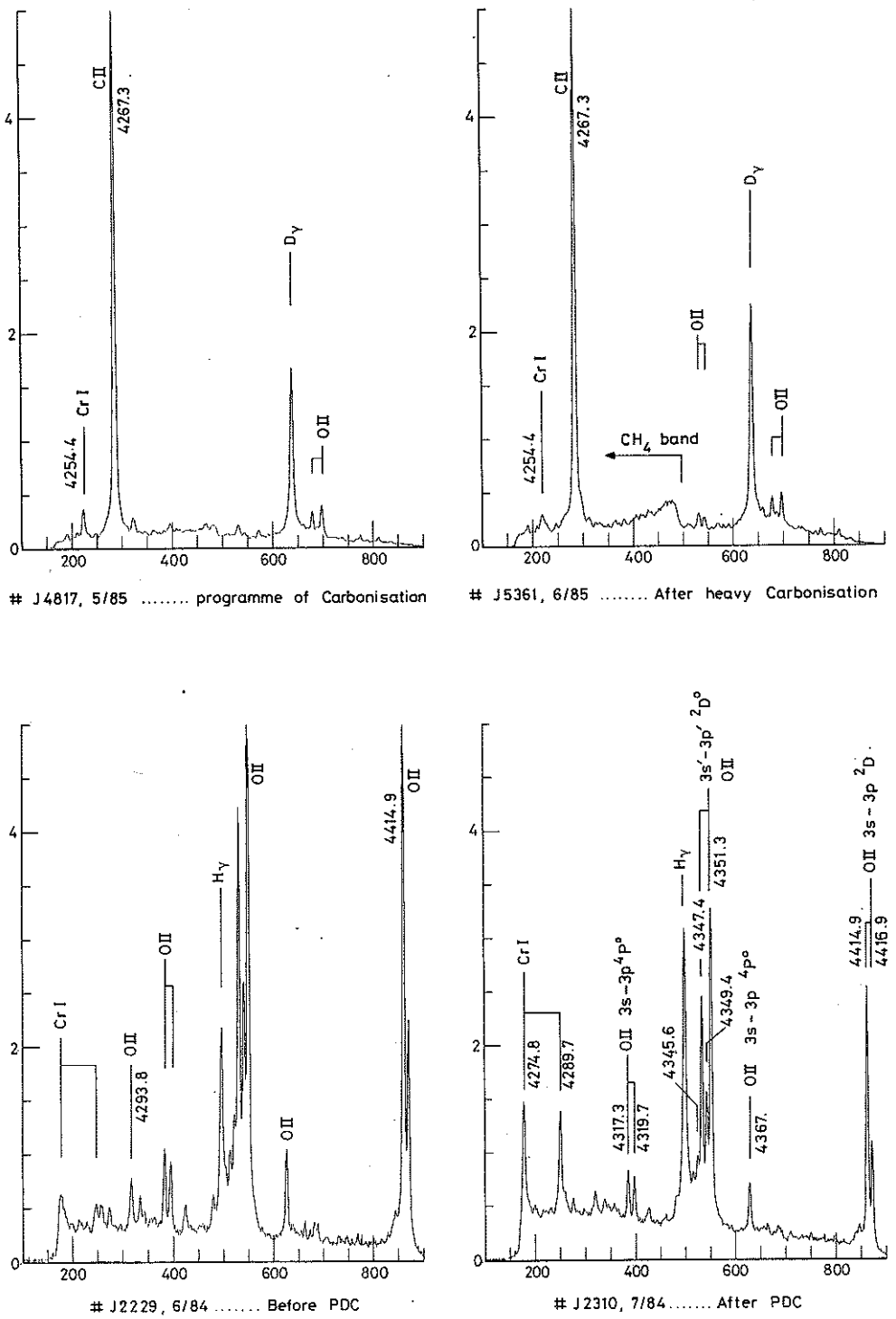

FIGURE 4

Spectrum from JET in the region of Balmer γ. The intensities of the OII multiplets, the Cr I triplet and C II at 4267.3 Å relative to the intensity of Hγ are commonly used for deriving influxes of impurities. The influx ratios of these impurity ions relative to that from hydrogen changes, as illustrated, with torus wall conditioning. The term 'PDC' means pulse discharge cleaning. 'Carbonisation' results from glow-discharge cleaning in methane.

TABLE 1

Deployment of Optical Fibre Conducts on JET

PERIOD	NO OF OPTICAL FIBRES IN USE ON JET	PURPOSE
JUNE 83	3	$H\alpha$, TOTAL LIGHT AND BREMSSTRAHLUNG SIGNALS AT UPPER AND LOWER WALLS
OCT-DEC 83	10	FURTHER MONITORING OF UPPER AND LOWER WALLS (AT EACH OCTANT) AND VIEWS ON 2 LIMITERS [$H\alpha$, BREM., CIII, OII, OIV, NiXII, ETC].
1984-85	14	ADDITIONAL VIEWS OF LIMITERS, ICRH ANTENNAE AND INNER WALL.
1986-	30	ADDITION OF MULTICHORD ARRAY (13) IN 1986 IN ONE POLOIDAL CROSS-SECTION, VIEWS OPTIMISED FOR C/X MEASUREMENTS IN BEAM-HEATED PLASMAS.

TYPE OF FIBRE - Q & S F-1000W (POLYMER CLAD SILICA (PCS) ie, HIGH OH CONTENT OR 'WET' TYPE)

CORE DIAMETER	1MM
APERTURE	0.3 RAD
PASSBAND	3500Å - 11000Å
ATTENUATION	8dB/km at 6500Å

IV Balmer Emission

As is common in tokamak studies, the Balmer emission from hydrogen and its isotopes has been interpreted in JET in terms of an ionisation model of the atoms as they leave the material walls or limiters and penetrate the plasma boundary. From the radiance Φ (photons $cm^{-2}st^{-1}s^{-1}$) of the Balmer lines, the input flux of ions is approximately

$$\Gamma_{H^+} = 4\pi \frac{\bar{S}_{H^\circ} \Phi_{H^\circ}}{\bar{X}_{H^\circ B}} \qquad (4)$$

S being the total ionisation coefficient, X the effective excitation coefficient to the upper level of the transition and B is the branching ratio. A correction has to be included for the break up of the H^+_2 molecule without H_α emission. From the electron density profile $n_e(r, t)$ measured in JET by multichannel FIR (DCN Laser) interferometry, and with absolute influxes integrated over the plasma boundary surface, then the global electron confinement can be derived using particle balance, equation (2). In practice the influxes of impurities contribute to the plasma electrons as also does the injection of high energy H° and D° beams and other extraneous refuelling methods.

The particle confinement [13] [14] depends critically on the operating conditions. A sample time history with atomic beam injection and an 'X-point' magnetic flux boundary is shown in Fig.5. The loss in confinement during the X-point formation and its transient recovery when the plasma adopts an 'H-mode' are well illustrated.

The recycling rate of atomic hydrogen at the material boundary is related to the loss rate by

$$\bar{S}_{recycl} = \frac{R\,\bar{n}_e}{\bar{\tau}_p}$$

and the density change in the plasma is then

$$\frac{d\,n_e}{dt} - (1-R)\,\frac{\bar{n}_e}{\tau_p} = \sum (S_g + S_p + S_b + S_i) \qquad (5)$$

where $\sum$ includes the contribution to the electron density from gas feed at the boundary, S_g, from solid pellet injection, S_p, from atomic beams, S_b and from impurities, S_i. In the general case for $R \neq 1$, a solution of (5) is

$$n_e(t) = \sum(S)\,\frac{\tau_p}{(1 - R)}\,\{1-e^{-(1 - R)t/\tau_p}\} + n_e(0)e^{-(1 - R)t/\tau_p} \qquad (6)$$

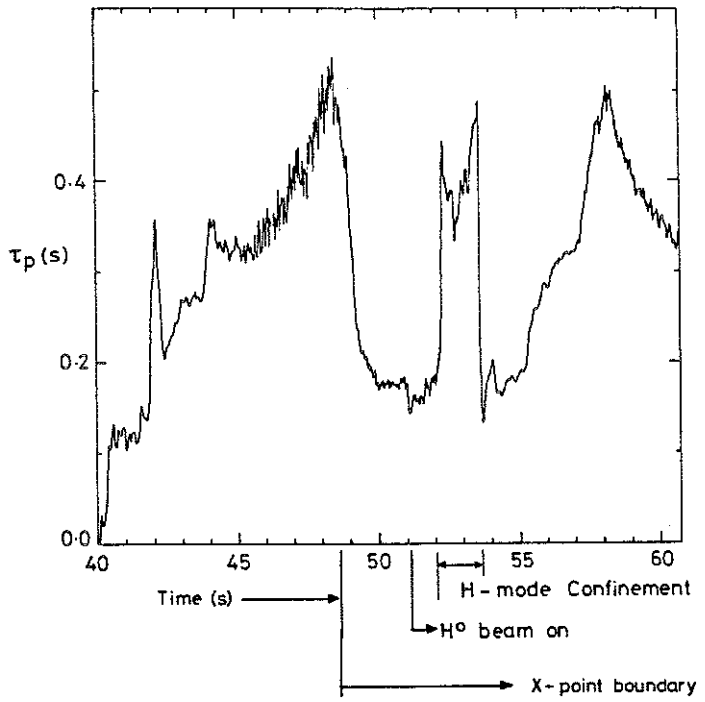

FIGURE 5

Temporal variation of global particle confinement time τ_p (J #10789). The figure illustrates the complex variation in τ_p as the plasma is relocated inside the torus from contact with a limiter boundary to a magnetic, X-point boundary (at 49s). Following switch-on of neutral beams (~51s) the plasma adopts a transient (1.3s duration) higher confinement (H-) mode.

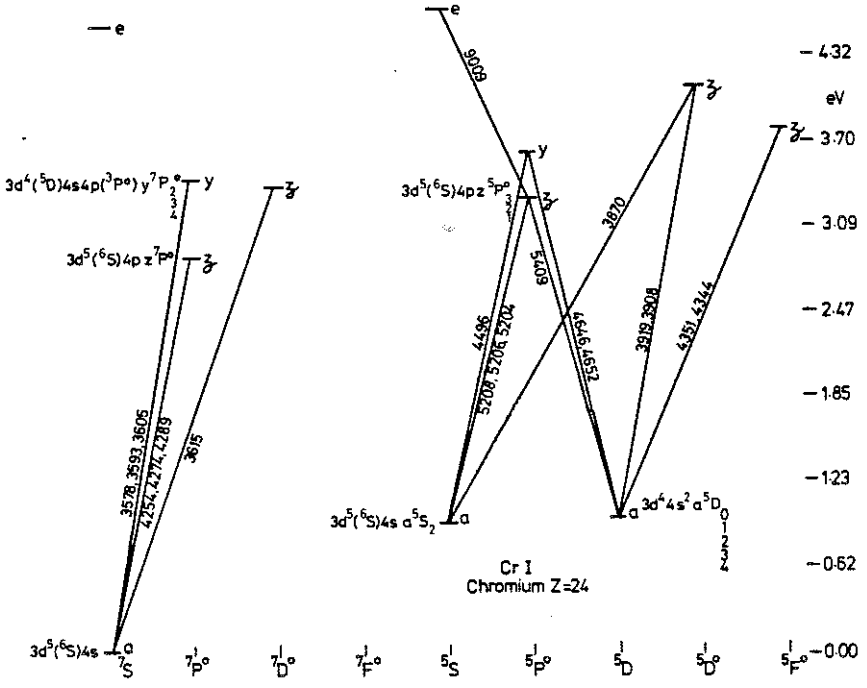

FIGURE 6

Grotrian Diagram of Cr I.

For the particular case of $\sum(S) = 0$, this equation reduces to

$$n_e(t) = n_e(0)\ e^{-t/\tau^*} \qquad (7)$$

where, $\tau^* = \tau_p/(1 - R)$. The absolute value of τ_p is of no particular significance since it represents neither an average particle confinement time nor a confinement time for the central ions. However, the concept of τ_p and τ^* and their variation with $\bar{n}_e$, all other plasma conditions being kept constant at a given time reference, can provide a useful insight into transport mechanisms [7] [8]. Also, a knowledge of the variation of τ_p and τ^* during a discharge is a prerequisite to obtaining effective density control, for example during the current ramp-down period at the end of the discharges. In 'standard' JET discharges, with ohmic heating, fuel recycling at the carbon limiters is the main source of electron influx during the current plateau and $R \simeq 1$, [13], [14].

The Balmer radiances (see eg, Fig.2) are also used to monitor isotope (H° and D°) exchange [14] when transferring from one fuel species to another.

Impurity Influxes

The Balmer spectrum, Figs.2-4, is interspersed with, even sometimes dominated by, line radiation from neutral and weakly ionised atoms of impurities, the most persistent of which have been the light elements carbon, oxygen and chlorine with the metallic constituents which make up the inconel (Ni - alloy) wall material. It happens that strong multiplets of these elements often lie close to the members of the Balmer series and the radiances of the impurities relative to the Balmer lines provides a good first indication of the impurity influxes relative to the fuel influx. Figure 4, for example, shows the variation of the intensities of the OII multiplets at the carbon limiter relative to H_γ under various tokamak operating conditions. These OII transitions underline a subsidiary problem relating to the atomic physics model used in the calculation of $\frac{S}{X}$ in the influx formula (4). The strongest OII transitions shown, Fig.4, are

3s - 3p ^2D, 3s´ - 3p´ ^2D and belong to the metastable doublet system rather than the quartet ground state system. Calculations by Summers et al, [15] also [16], [17], indicate that excitation within the metastable system is more likely than intersystem excitation and that appreciable inward transport of OII occurs in the metastable state, see table II. An example of the metal influxes, namely Cr I, is also shown in Fig.4, where the septet lines from the resonance decay of the $3d^5(^6S)4pz^7p^\circ$ levels of Cr I, Fig.6, are often a measurable feature in the proximity of H_γ. In contrast, the quintet system lines arising from the ^5S and ^5D metastables are weak relative to the septet lines. Metastable states therefore make no appreciable correction to the calculated influxes in the case of Cr I. The problem of metastable influxes has not been solved in general and each ion or atom as in the calculations of Summers et al [15] has to be considered individually. The variations of $\frac{S}{XB}$ for several atomic and ion species used for influx calculations in the JET studies [9], [16] are shown as a function of T_e in Fig.7. The 4254 Å line of Cr I is particularly convenient since every photon means approximately one ionisation event at the high edge temperature in JET where $T_e \sim 100eV$.

Clearly, using the same arguments as for the fuel particle balance, the impurity ion balance and confinement time can also be derived [8], [9] provided that reasonably accurate values of the central impurity ion concentrations are available.

Identifying the total influx as

$$\int_{area} \Gamma_A . da = \int_{vol} \frac{\sum n_{A^+}}{\tau_A} . dv$$

where the volume integral is summed over all ion stages, then, from (3),

$$\frac{\tau_A}{\tau_H} = \frac{(\lambda_i + \lambda_{sol})_A}{(\lambda_i + \lambda_{sol})_H} \qquad (8)$$

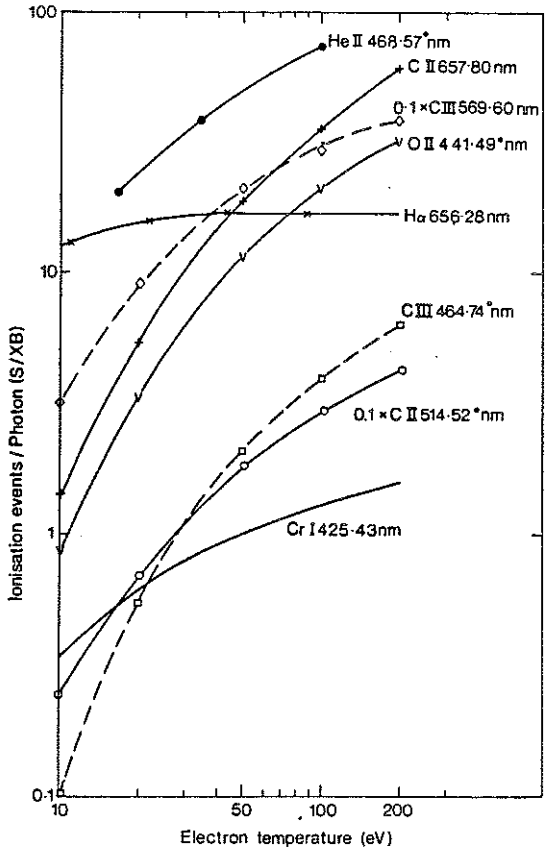

FIGURE 7

Ionisation events per photon for some impurity lines used for calculating atomic and ionic influxes as a function of electron temperature. The starred transitions are those predominantly populated from a metastable level.

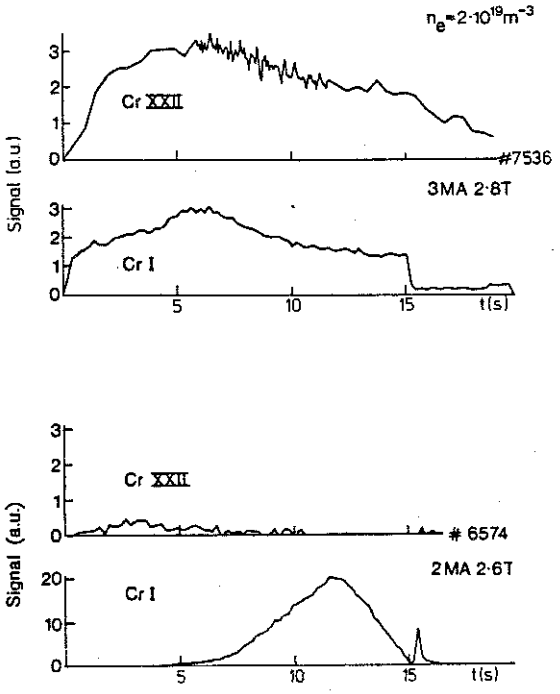

FIGURE 8

The upper pair of line intensities (J #7536) indicate a good correlation between influx rate of Cr I and the Cr XXII concentration in the body of the plasma as expected for physical sputtering at the limiter. In contrast, with evaporation of Cr I from the limiter on JET pulse J #6574, there is no correlation between the time histories of the influxes (proportional to the intensity of Cr I) and the chromium concentration in the plasma (proportional to the intensity of Cr XXII).

TABLE II

Oxygen ion, OII, influxes (from limiter) in metastable states and ground state (under-lined) compared to hydrogen influxes (J # 5368, 5372, 5374)

Ion	Wavelength (Å)	S/XB (T_e = 100 eV)	Γ'_O/Γ_H in a particular state	Γ_O/Γ_H (%)
O II	3749.5	53	0.74% in $2s^22p^3\ {}^4S^0$	
	3973.3	35	0.25% in $2s^22p^3\ {}^2P^0$	
	3912.0	≈ 73	≈ 0.22% in $2s^22p^3\ {}^2P^0$	1.6
	4414.9	28	0.60% in $2s^22p^3\ {}^2D^0$	
	4351.3	≈ 35	≈ 0.62% in $2s^22p^3\ {}^2D^0$	

Typically this ratio exceeds unity due to the relatively high energy (tens of eV) with which some H° atoms are born from resonance charge-exchange collisions at the plasma edge and the Frank-Condon (few eV) dissociation energy of H^+_2 released from the material boundary. In contrast, the release energies of the metals by physical spluttering are ~ 1eV. Typically then for JET, the ratio, equation (8), is about 0.1 with global confinement of the metal impurities ~ 10ms. Dramatic evidence for the relation between influx energy and global confinement is seen in relatively clean discharges where the torus has been freshly pre-conditioned by glow discharge cleaning in methane (carbonisation). In such discharges electron heat loss causes the temperature of the material limiters to rise until chromium atoms are released by evaporation. The release energy of CrI, in this case ~ 0.1 eV , is insufficient for the chromium atoms to penetrate the plasma boundary. Despite the large increase in the observed CrI brightness at the limiter surface, Fig.8, there is no concomitant increase in the Cr contamination in the body of the plasma.

Spectral Shapes of Edge Lines

Other spectroscopic studies [18] of edge plasma phenomena relate to the measurement of plasma instabilities including the formation of poloidally asymmetric high density regions [19], so called MARFE's, which occur near

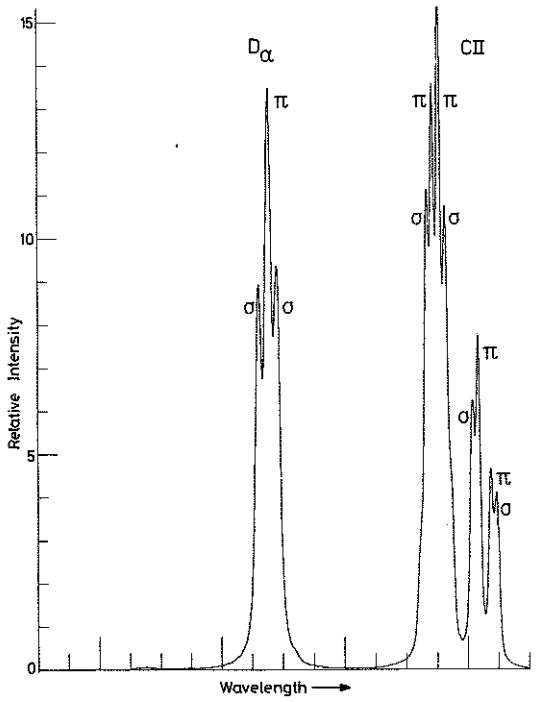

FIGURE 9

Spectrum in region of Balmer α from JET plasma in contact with inner wall during termination phase of JET discharge (J #11041). Magnitude of Zeeman splitting confirms the location of the plasma edge inside the torus. The relative line intensities and the line splitting are in marked contrast to spectruum shown in Fig.2.

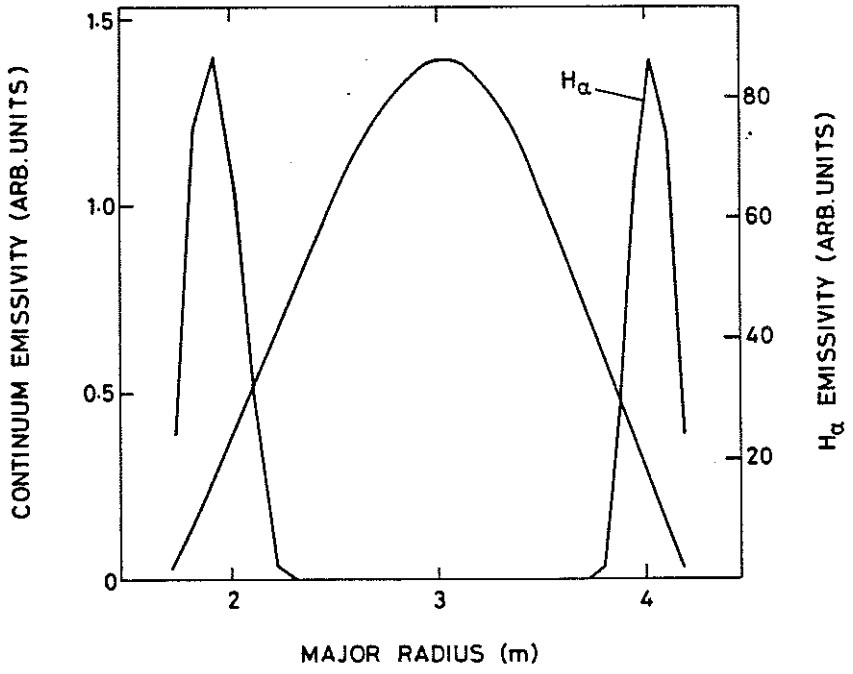

FIGURE 10

Radial distribution of the emissivity of Hα (J #10850) compared to the continuum emissivity (J #9376) at 5235 Å. The data are schematic to the extent that the intensities are on approximately the same arbitrary scale and the Hα peaks have an exaggerated width due to the limited spatial resolution of the array of viewing chords.

the maximum operational density limit in a tokamak. These relatively high density cool regions are characterised by enhanced local brightness in the line emission from low ion stages eg, CIII.

The 'launch' energy of the influxing atomic species, as we have described above, is an important factor in the trapping and global confinement of the particle species in a tokamak. Attempts are now being made on JET to measure the injection energy of H^0, CII, HeI, HeII at the plasma edge using an échelle spectrometer and OMA detection system with an overall resolving power $\frac{\lambda}{\delta\lambda} \sim 10^5$. Preliminary results, as expected, indicate considerably higher launch velocities for H^0 than for the light impurity atoms. A noticeable feature of the atomic spectra is the Zeeman splitting due mainly to the toroidal magnetic field which scales inversely as the major torus radius, $B_\phi \propto R^{-1}$. The magnitude of the Zeeman splitting uniquely locates the atomic or ionic shell [20] and allows us to discriminate between material excited at the inner or outer material boundary or at the plasma edge, these locations being not necessarily coincident. An extreme example of the Zeeman split lines of $H\alpha$ and its neighbouring CII doublet is shown in Fig.9. The magnitude of the splitting confirms that the plasma is in contact with the inside wall, R = 2.11 m during the time frame following a disruption to the current and subsequent loss of the plasma equilibrium.

V CHARACTERISTIC VISIBLE EMISSION FROM THE PLASMA CORE

The Effective Ion Charge State

It is found convenient to define a parameter as

$$Z_{eff} = \frac{\Sigma n_i z_i^2}{\Sigma n_i z_i} \qquad (9)$$

where Z_{eff} is the effective ion charge 'sampled' by the electrons during coulomb collisions. Z_{eff} appears in expressions for the electrical conductivity and for the bremsstrahlung emission, both of these plasma

parameters depending essentially on coulomb collisions between ions and the free electrons in the plasma. Differences between the resistive and radiative Z_{eff} are often meaningful to plasma physicists in terms of anomalous collision processes, trapped particles and non-Maxwellian energy distributions. Only in the case of classical electron-ion collisions in a field free plasma should these Z_{eff} parameters be equal.

In the case of the bremsstrahlung continuum [21] the power spectrum (photons cm^{-3} A^{-1} s^{-1}) is given by

$$P_{Bremss}(r) = 9.5x10^{-14}\ \lambda^{-1}\ g_{ff}\ n_e^2(r)\ Z_{eff} T_e^{-\frac{1}{2}} \exp\left(\frac{-hc}{\lambda k T_e(r)}\right) \qquad (10)$$

In the visible region with $h\nu << kT_e$ but where free-free absorption is not an issue, the intensity is weakly dependent on temperature. The free-free collision, quantum mechanical correction factor g_{ff} is usually greater than unity, typically ~ 3, and is a function of $h\nu/kT_e$ and Z_{eff} [22]. The bremsstrahlung radiance, of course, integrates the free-free emission along a chord through the plasma and is biased towards the high density region in the core. For this reason an array of line-of-sight chords in the poloidal plane is used to evaluate the local continuum emissivity. Figure 10, illustrates the contrast between the spatial variation of the visible continuum intensity and that from H_α. The continuum emission is measured at 5235Å over a bandwidth of 10Å, this region of the spectrum having been identified by the OMA survey spectroscopy as free of competing line emission from the plasma edge, Fig.11. Even so, the band-width integrated continuum radiance ~ 10^{11} photons cm^{-2} s^{-1} str^{-1} is at least two orders of magnitude weaker than line radiances from recycling fuel atoms. Recent results using the poloidal array diagnostic has indicated that for most discharge conditions $Z_{eff}(r)$ is a smoothly varying functions with plasma radius. Under favourable conditions therefore, the $Z_{eff}(r)$ monitor may be used to interpolate $n_e(r)$ from equation (10) with better spatial resolution than that achieved with multi-channel FIR interferometry.

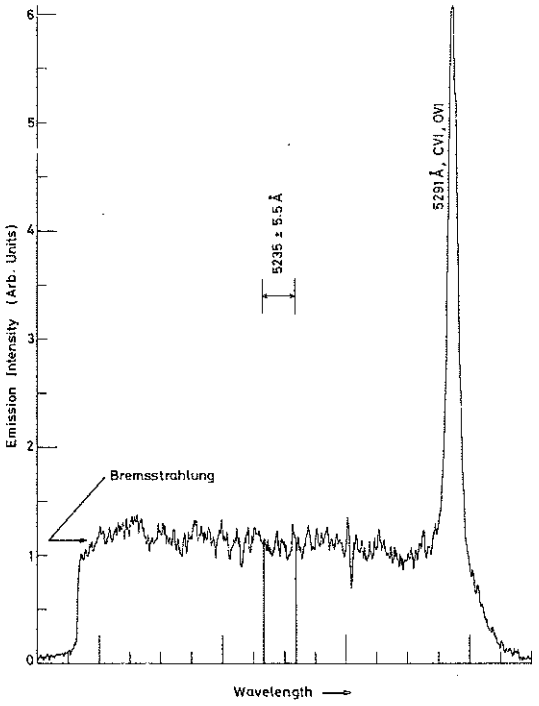

FIGURE 11
Spectrum around 5235 Å showing limited line-free region used for measurements of bremmstrahlung intensity (J #8965). The detector dark current corresponds to ~ 0.4 on the intensity scale. The n = 7-8, transition in CVI at 5291 Å, which is used in the CXRS analysis, shows only a 'cold' component since the viewing chord intersects no part of the plasma volume which is irradiated by neutral beams.

Forbidden Lines from Highly Ionised Metals

The line spectrum from L-shell ions of the common metals Ti, Cr, Fe, Ni etc includes magnetic dipole and intersystem transitions with $2s^k 2p^\ell$ ground configurations [23]. These $\Delta n=0$ transitions lie, in general, at long wavelengths in the quartz UV or visible spectral regions and they have been used in the past for measuring some of the characteristics of the core plasma in tokamaks. A typical radiance for these lines with about 0.5% ionic concentrations relative to n_e is $\sim 10^{13}$ photons s^{-1} cm^{-2} str^{-1}. These relatively high metallic ionic concentrations are available with laser ablation techniques [23]. However the intensities of these forbidden lines depends critically on the electron collisional de-excitation rate

relative to their spontaneous decay rates and over the range of densities covered by most tokamaks these rates are of the same order [24]. At electron densities $n_e \gtrsim 10^{14}$ cm^{-3} the forbidden lines are often blended with the background emission. Unfortunately also, nearly all the lines lie at wavelengths shorter than the fibre-optic transmission cut-off and so become unusable with the present JET optics. The intrinsic concentrations of metal impurities in JET has typically been << 0.1% of n_e in standard discharges with $\bar{n}_e \sim 3 \times 10^{13}$cm^3 so that it is not surprising that forbidden lines from the core have not been observable features. Several M1 forbidden lines of Ni e.g. NiXXIV at 609.6Å have been observed however in the VUV region, and since controlled injection of metals by laser ablation is now planned for the next operational phase on JET then diagnostics based on forbidden lines from the L-shell ions of metal may still be viable. There are several possibilities for M1 lines from M-shell ions, for example the ground term $^2P_{1/2-3/2}$ splitting of the ClI sequence [25]. These M-shell ions are of limited use in diagnosing the core plasma however, since they are located near the plasma boundary in JET. The same comment applies to the NiXII line at 4231Å which is the only prominent forbidden metal line already observed in the visible spectrum from JET.

CHARGE EXCHANGE RECOMBINATION SPECTROSCOPY (CXRS)

Since early 1986, advantage has been taken of the neutral particle heating beams (H^0 or D^0 at particle energies of $\lesssim$ 80 keV) to introduce on JET a diagnostic based on the spectral signature of the reaction

$$H^0 + Z^{+z} \rightarrow H^+ + [Z^{+(z-1)}]^*$$

The starred quantity indicates electron capture into an excited state with principle quantum number 'n'. Cascade de-excitation of the recombined nucleii Z^{+z} results in the emission of predominantly $\Delta n=1$, lines some of which lie in the visible region [26]. Charge exchange recombination lines (CXR) which lie in the visible region and which have proved useful in the JET beam heating programme during 1986 include H_α and H_β at 6563Å and 4862Å

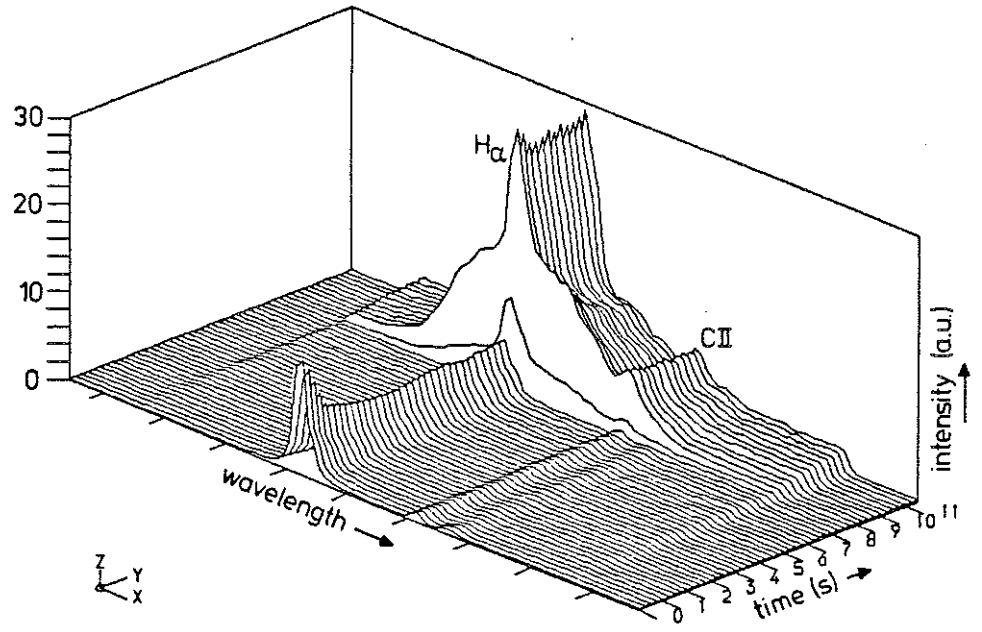

FIGURE 12

Spectrum of Balmer α viewed along a vertical chord which intersects the horizontal trajectory of the atomic (H° or D°) heating beams in JET. The beam current is switched on at 7.5s during discharge #J7145.

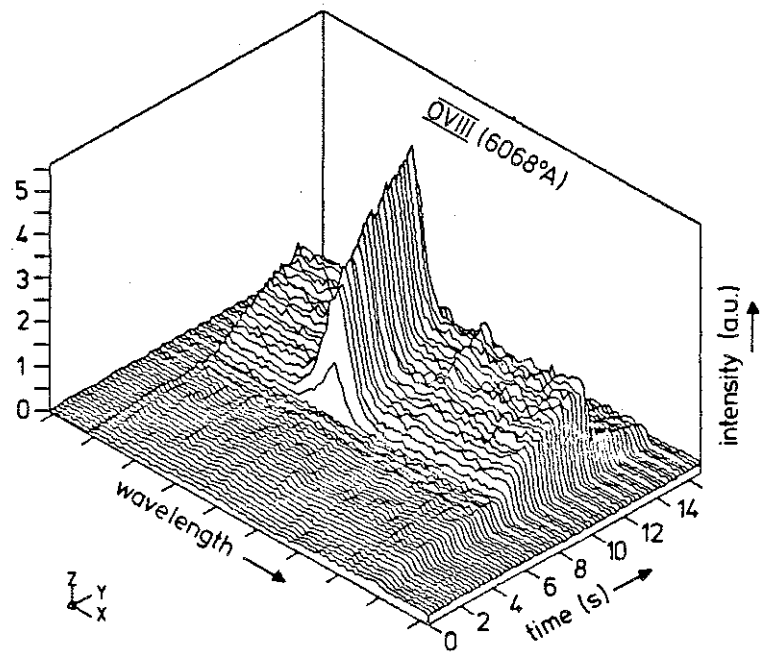

FIGURE 13

Time history of n = 9-10 transition in OVIII. The atomic beam is switched on at 8s, (J #7135).

respectively, HeII (n=3-4) at 4686Å; OVIII (n=9-10) at 6068Å and (n=8-9) at 4341Å; CVI (n=7-8) at 5291Å and (n=8-10) at 4500Å.

In order to observe these features the viewing chords must of course intersect the neutral beam trajectories through the plasma. In the CXRS experiments performed to date on JET the core plasma is viewed along a single vertical chord, see Fig.1, which intersects the horizontally directed beams at the minor axis (R=3.1m, r=0) while a second horizontal chord interesects the beams on the inner half of the plasma radius at R=2.3 m, r=0.8 m. Using only these two viewing chords it has been possible to derive a considerable amount of information on core ion temperatures, plasma rotation and concentrations of the light elements in JET [27], [28]. The signature of the CXRS lines is their large spectral width relative to other visible lines from the plasma edge combined with a strict time dependence on the neutral beam flux. These features are well illustrated Figs. 12 and 13 by the temporal and spectral evolution of H_α and of the OVIII 6068Å line during sample JET discharges. The observed spectra are usually composite profiles made up of a broad CXR component whose width is characteristic of multi-keV temperatures in the plasma core and a relatively narrow component consistent with emission from near the plasma edge. In the case of the oxygen lines, Fig.13, the edge components are negligible, in contrast to the CXR lines from the other light ions in JET, eg, Fig.12, which show edge emission throughout the discharge. Deconvolution of the broad high temperature component from the edge contribution, from other line blends and from the background continuum, as illustrated in Fig.14, is a necessary step in the analysis.

The spectral radiance of the broad component of the CXR lines can be related to the line-of-sight integral through the beam irradiated plasma,

$$\Phi_{CXR} = \frac{1}{4\pi} \int \varepsilon_{CXR}(\lambda)\, d\ell \qquad (11)$$

where,

$\varepsilon_{CXR}(\lambda) = \sum^{E_x} N(H^0)\, N(Z^{+z}) < \sigma_\lambda(n\ell,n'\ell')_{CXR} \bar{v}_b >$ and $\sigma_\lambda(n\ell,n'\ell')_{CXR}$ is the effective cross-section for excitation of the $n\ell$-$n'\ell'$ transition in the

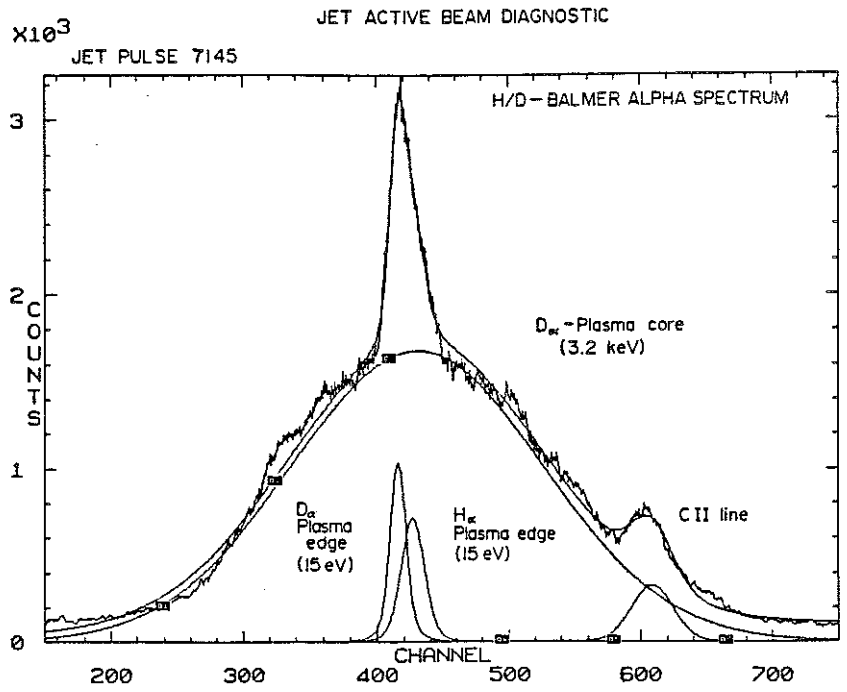

FIGURE 14

Example of deconvolution of Balmer α spectrum (Figure 12) excited by charge transfer recombination.

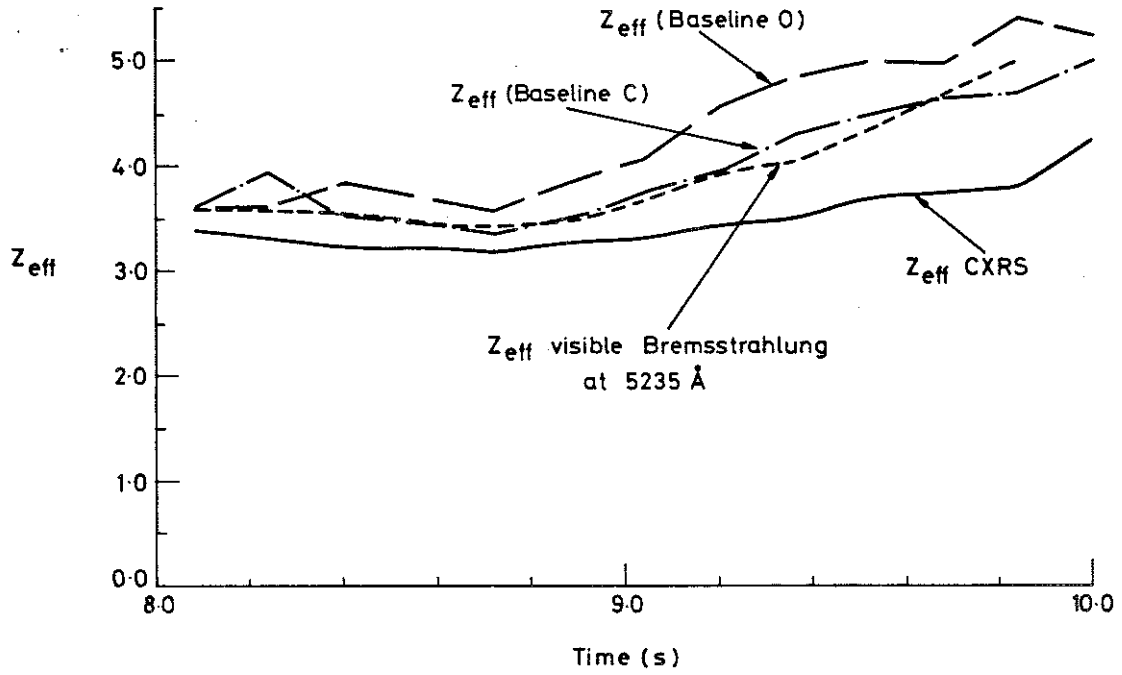

FIGURE 15

Effective charge state Z_{eff} derived from CXRS analysis of carbon and oxygen ions in centre of plasma, compared with bremsstrahlung continuum measurements in three regions of the visible spectrum.

recombined ion and $eN(H^0)\bar{v}_b$ is the neutral beam 'current'. The total emissivity, $\varepsilon_{CXR}(\lambda)$, is the sum over the separate energy components in the beam, E_x. Derivation of ion concentrations $N(Z^{+z})$ from equation (11) requires a certain amount of calculation. For example, the atomic beam attenuation is required in order to calculate local values for the density $N(H^0)$ of the beam atoms and their thermal biproducts, the so-called 'halo' neutrals [26], [29]. Fortunately the thermal halos make a negligibly small relative contribution (~ 1%) through charge-exchange, to the population of the high quantum states which radiate in the visible region of the spectrum of CVI and OVIII [29]. The effective atomic cross-sections for populating the states which contribute to the visible CXR line intensities are an on-going problem which involves an assessment of the validity of the basic (usually theoretical) cross-sections [26] as well as modelling the radiative decay routes with the inclusion of the state mixing due to the plasma environment [30]. The CXRS diagnostic offers the only direct method for measuring concentrations of completely stripped ions such as He^{2+}, C^{6+}, O^{8+} which at the multi-keV temperatures in JET occupy most of the plasma volume. The use of OMA detectors allows not only the intensities of the CXR lines to be recorded but also that of the neighbouring continuum. Since the main components of Z_{eff} are the fuel ions, (H^+, D^+ and also, on occasion, He^+), as well as the light impurities, principally oxygen and carbon, it is reasonable to construct Z_{eff} from its separate components measured by CXRS and compare this with the bremsstrahlung continuum Z_{eff}. In Fig.15 we compare Z_{eff} derived from the free-free continuum with Z_{eff} (r=0) due to the sum of the fuel and of the O^{8+} and C^{6+} impurity ion concentrations derived from CXRS. The continuum intensity has been measured at 5235Å and at the far wings of the CXR line profiles, the so-called 'base-line' continua in Fig.15. It is evident that the concentrations of the light impurities typically 4% of carbon and 1% oxygen relative to $\bar{n}_e$ in standard ohmic discharges, can account for most of Z_{eff} in JET. At a given n_e there is a tendancy for the main individual components of Z_{eff} to change around, depending on tokamak operating

conditions, while keeping the overall Z_{eff} constant. The residual Z contribution to Z_{eff}, Fig.15, can be ascribed to metal contamination, $<<0.1\%\ n_e$.

While the absolute radiance and spectral shape of the broad component of the CXR lines can be satisfactorily interpreted in terms of ion concentrations, thermal broadening and plasma rotation in JET)[27,28], it is more difficult to account for the relatively narrow edge component, particularly in the CVI ion emission. The low values of the effective CXR cross sections at impacting energies of < 1 keV/AMU discount charge transfer recombination of C^{6+} with thermal H^0 at the plasma edge as the explanation. Attempts are currently being made to account for the cold edge component in terms of other collision processes, such as CXR between C^{6+} and excited states of H^0 or electron impact excitation of blended lines of OVI [30].

CONCLUSIONS

From the very first year of JET operations, mid 1983 to 1984, when the available instrumentation restricted measurements to the visible and quartz UV region, a basic requirement from optical spectroscopy has been to identify the main impurity elements entering the JET plasma. Whilst identification of impurities remains a routine task, optical spectroscopy has assumed in recent years a more widespread significance in the JET programme. By relating the influxes to the core concentrations, through model calculations of the release of particles at the boundary and their diffusion into and out of the plasma, a general physical picture of the particle behaviour is emerging which may eventually allow us to rely entirely on visible data without appealing to spectroscopy at shorter wavelengths. An important factor in this scenario has been the development of visible CXRS for measuring the absolute local concentrations of bare nuclei which, incidentally, make up over 95% of the JET plasma. Coupled with the capability for measuring the brightness of the visible continuum and therefore Z_{eff}, visible spectroscopy becomes almost self-sufficient as a diagnostic for studying impurity and fuel particles. It should be added

though, that diagnostics such as bolometry which provide spectrally-integrated radiation levels, will always provide a reassuring check on the visible data.

Looking to the future phases of the JET programme when fusion-burn (D-T) plasmas are contemplated then spectroscopic diagnostics will be faced with new technical problems originating from the radioactive environment. Vacuum spectroscopy with instruments close-coupled to the torus will become inoperable due to neutron activation and neutron induced detector noise. Over the last two years of operation in JET up to 10^4 pulses with 10^{20} neutrons over a 20s pulse can be anticipated. Under this irradiation, even remotely coupled visible spectroscopy will have problems since the attenuation of the quartz fibres at 6500Å can reach 15dB and can be as high as 30dB at 4000Å. Solutions contemplated, however, include photo-bleaching between JET discharges or regularly renewing those critical few metres of fibre close-coupled to the torus or even replacing them with mirror relay optics [5]. It is anticipated therefore that degradation of the optical fibre transmission due to neutron irradiation can be circumvented. In these circumstances the prospects are that visible spectroscopy, with spectrometers operated remotely from the torus, will remain viable throughout the JET programme and will become an essential diagnostic.

REFERENCES

[1] Rebut P H et al. Proc. of 11th Int. Conf. on Plasma Physics and Controlled Fusion Research (Kyoto, Japan) Nov. 1986 - see JET preprint P-(86)44.

[2] Cordey J G et al, Ibid (1986).

[3] Barnsley R, Fielding S J et al. Culham Laboratory Pre-print CLMP-792 (1987).

[4] Anashin A M, Gorbunov E P, Ivanov D P, Lysenko S E, Peacock N J, Robinson D C, Sannikov V V and Strelkov V S. Soviet Phys. JET P, 33, No 6. 1127-1133 (1971).

[5] Morgan P D, Behringer K H et al. Rev. Sci. Instru. 56 (5). 862-864. (1985).

[6] Engelhardt W W. 'Wall Effects and Impurities on JET'. Proc. Roy. Soc. Meeting. London (1986). JET Preprint JET-P(86)27.

[7] Engelhardt W W and Feneberg W., Jnl. Nucl. Materials. 76 and 77, 518-520 (1978).

[8] Engelhardt W W et al., Jnl. Nucl. Materials. 111 and 112. p337 (1982).

[9] Behringer K H. 'Spectroscopic Studies of Plasma-wall Interaction and Impurity Behaviour in Tokamaks'. Proc. 7th Int. Conf. on Plasma Surface interactions in Controlled Fusion Devices. (Princeton) 1986. Jnl. of Nuclear Materials (145-147), pp 145-153 (1987).

[10] Lackner K and Post D E. Proc. NATO Summer School (Val Morin, Canada) (1984).

[11] Behringer K H, Carolan P G, et al., Nuclear Fusion. 26, No.6. 751-768. (1986).

[12] Johnson L C and Hinnov E., Jnl. Quant. Spect. and Radiative Transfer. 13. 333-358. (1973).

[13] Cheetham A, Christiansen J P, et al., 'Electron Density Transport in JET'. Proc. 13th Euro. Conf. on Controlled Fusion and Plasma Heating (Schliersee). Vol. 10C part 1, 240-243.

[14] Morgan P D, Corti S, et al. 'Recycling, Isotopic Exchange and Density Behaviour in JET Discharges'. Proc. 12th Euro. Conf. on Controlled Fusion and Plasma heating (Budapest, 1985), Vol.9F, part II, 535-538.

[15] Summers H P, Behringer K H, et al. 'Interpretation of emission from ions out of ionisation balance'. JET-P(86)42.

[16] Stamp M F, Behringer K H, et al. 'Impurity Sources and Impurity Fluxes in the JET tokamak'. Proc. 12th Euro. Conf. on Controlled Fusion and Plasma Heating, (Budapest, 1985), Vol.9F, part II, 539-542.

[17] Stamp M F, Behringer K H, et al. 'Impurity Influx Behaviour in JET'. Proc. 7th Int. Conf on Plasma Surface Interactions in

Controlled Fusion Devices, (Princeton) 1986. Jnl. of Nucl. Materials (145-147): 236-240 (1987).

[18] Carolan P G, Forrest M J, Hawkes N C and Peacock N J. 'Studies of Edge Phenomena in JET with visible Spectroscopy'. Proc. of 12th Euro. Conf. on Controlled Fusion and Plasma Physics. Budapest (Sept. 1985) Part 1. 9F. pp 263-266.

[19] O'Rourke J, Campbell D, Denne B, et al., Proc. 12th Euro. Conf. on Controlled Fusion and Plasma Physics. Budapest (Sept., 1985). Paper 190. See JET Pre-print JET-P(85)10. pp 81 (1985).

[20] Carolan P G, Forrest M J, Peacock N J and Trotman B L., Plasma Physics and Controlled Fusion, 27, No.10, pp 1101-1124.

[21] Foord M E, Marmar E S and Terry J L., Rev. Sci. Instr. 53 (9), 1407-09 (1982).

[22] Karsas M J and Latter R., Astrophys. J. (Suppl) 6, 167 (1961).

[23] Finkenthal M, Bell R E and Moos H W., J. Appl. Phys. 56 (7) 2012-16 (1984).

[24] Feldman U, Doschek G A, Cheng C C and Bhatia A K., Jnl. Appl. Phys. 51, 190-201 (1980).

[25] Suckewer S, Hinnov E, Cohen S, Finkenthal M and Sato K. PPPL-1899. May 1982.

[26] Carolan P G, Duval B P et al., Physical Review, A. April 1987.

[27] Von Hellerman M G V, Engelhardt W W et al. 'First Spectroscopic Charge Exchange Measurements During Neutral Injection on JET'. Proc. 13th Euro. Conf. on Controlled Fusion and Plasma Physics Schliersee. Vol.10C. Part 1, 120-123 (1986),

[28] Von Hellerman M G V et al., Proc. of Workshop on high temperature plasma Diagnostics. Varenna. See JET preprint, JET-P(86)45, pp64. (1986).

[29] Fonck R J, Darrow D S and Jaenicke K P., Phys. Rev. A. 29, No.6, 3288-(1984).

[30] Boileau A et al. JET Preprint (to be published, 1987).